

Supporting Information:

Characterizing the Stability of Ultra-Thin Metal Oxide Catalyst Films in Non-thermal Plasma CO₂ Reduction Reactions

Samuel K Conlin¹, Joseph Joel Muhanga², David N. Parette¹, and Robert H. Coridan^{1,2*}

¹Department of Chemistry and Biochemistry, University of Arkansas, Fayetteville AR, 72701, USA.

²Materials Science and Engineering Program, University of Arkansas, Fayetteville AR, 72701, USA.

*Email: rcoridan@uark.edu

Atomic Layer Deposition Parameters for the Growth of TiO₂ and ZnO on n⁺-Si Wafers with Native Oxide Layers:

A roughly 20 nm thick layer of TiO₂ was grown directly on the n⁺-Si substrate from tetrakis(dimethylamido)titanium (abbreviated TDMAT, 99%; Strem) and water under a continuous flow of 20 sccm of N₂, metered by a mass flow controller at 390 mTorr base reactor pressure, and 150 °C growth chamber and chamber door temperature. To deposit TiO₂, the substrates were placed inside the ALD chamber and exposed to 404 cycles of TDMAT and H₂O, with a 45 second purge time between precursor and water exposure. Each cycle consisted of an exposure to TDMAT (100 ms), a purge step (45 s), an exposure to water (21 ns), and a final purge step (45 s). A roughly 20 nm thick layer of ZnO was also grown directly onto n⁺-Si substrates under the same chamber flow, pressure, and temperature conditions as TiO₂. To deposit ZnO, the substrates were placed inside the ALD and exposed to 123 cycles of diethylzinc (DEZ, 95%; Strem) and H₂O, with a 45 second purge time between precursor and water exposure. Each cycle consisted of an exposure to DEZ (21 ms), a purge step (45 s), an exposure to water (21 ms), and a final purge step (45 s). Once deposited, the samples were removed from the ALD and stored in air before being analyzed and used as prepared.

X-ray Photoelectron Spectroscopy (XPS) of as-prepared, Thermally Annealed, and CO₂ Plasma Exposed ALD-TiO₂ and ALD-ZnO Films:

Samples of ALD-MO_x catalysts for XPS were prepared both before and after plasma exposure by removing small sample fibers from the interior of the support and placing them on a sample holder via conductive carbon tape. This holder was then stored in air for 24 hours prior to measurement. The data was collected with a PHI Versaprobe XPS and analyzed using the CasaXPS software suite. Background subtraction was performed using the CasaXPS default sigmoidal-type *Shirley* method around the region of interest. Peak fitting was performed using the CasaXPS *Marquardt* peak type, and automatic fitting refinement was performed iteratively until the residual standard deviation from the measured data was minimized with the minimum number of peaks included.

Debye-Scherrer Analysis for the Estimation of Crystallite Size on ALD-synthesized TiO₂ and ZnO Films:

The average crystallite size of the as-deposited, thermally annealed, and plasma exposed films was estimated from the most intense x-ray diffraction (XRD) Bragg reflection using the Debye-Scherrer Equation (Equation S1),^{1,2}

$$l = \frac{k \lambda}{\beta_{sample} \cos(\theta)}, \quad \text{Equation S1}$$

where l is the average crystal size in nm, k is Scherrer's constant taken as 0.93, λ is the wavelength of Cu K α X-ray source (0.15406 nm), β_{sample} is the FWHM of the XRD peak in radians sans instrumental broadening and $\cos(\theta)$ is the diffraction angle of the indexed peak in radians.

The indexed Bragg reflections were fit to a Gaussian function, $g(x)$, to estimate the FWHM, as described in Equation S2,

$$g(x) = \frac{1}{\sqrt{2\pi}\sigma} e^{-\frac{(x-x_0)^2}{2\sigma^2}}, \quad \text{Equation S2}$$

where x_0 is the mean of the gaussian fit and σ is the width. The calculated σ is then used to calculate β_{peak} , as shown in Equation S3.

$$\beta_{peak} \approx 2.355 \sigma_{peak} \quad \text{Equation S3}$$

The calculated β_{peak} is then used to determine the broadening associated with the crystal size, β_{sample} , using the experimentally determined instrumental broadening, Equation S4.

$$\beta_{sample} = \sqrt{\beta_{peak}^2 - \beta_{Instrumental}^2} \quad \text{Equation S4}$$

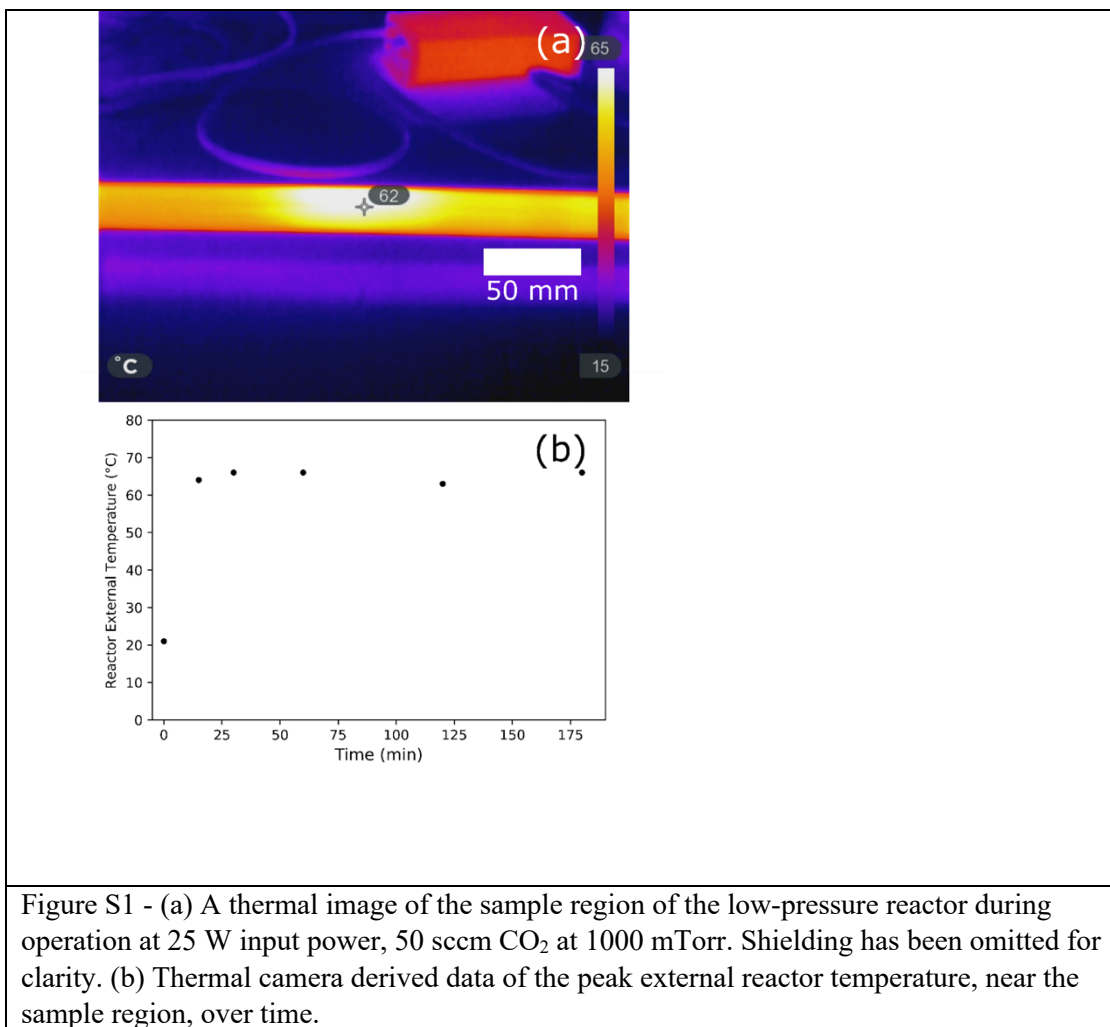


Figure S1 is a thermal camera image of the exterior of the reactor taken during the plasma-on period. The emissivity was compensated for natively and used by the camera to determine the temperature of the outside of the quartz tube. The temperature of the outside of the quartz tube at the sample region is reported as a function of time, with the temperature remain below 70°C throughout the plasma-on time. The low reactor temperature and bulk gas temperature were insufficient to thermally annealed the films by temperature only during plasma exposure, as this was lower than the ALD deposition temperature. This means that any changes in morphology were due to surface-plasma interactions.

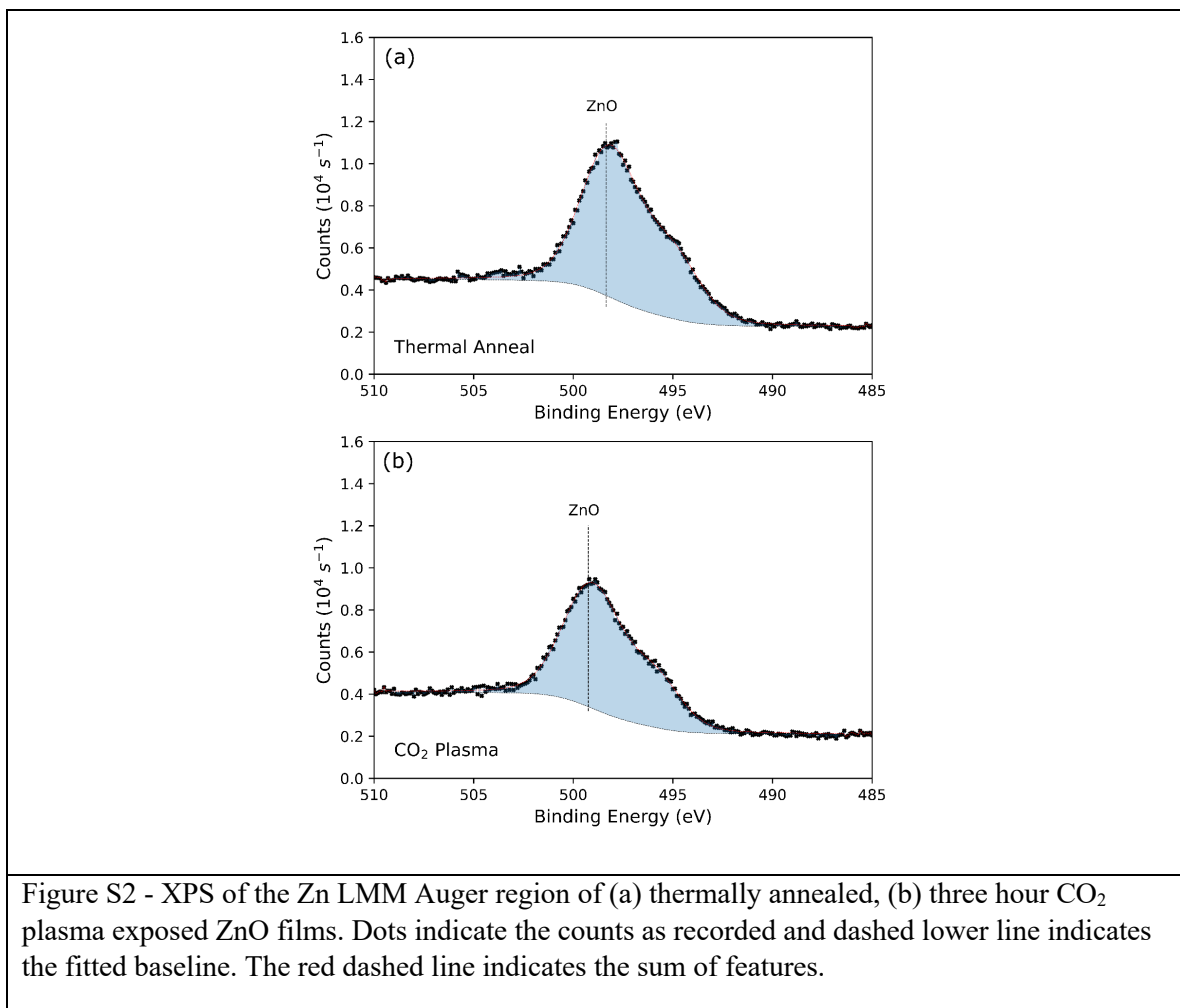


Figure S2 shows XPS spectra of the ZnO LMM region, showing the feature associated with ZnO after thermal annealing and CO₂ plasma exposure. The comparison between spectra and the lack of a resolved feature at 493.3 eV indicates that there is negligible difference in the surface chemistry of each sample. Therefore, there is no evidence of stable, reduced Zn¹⁺ and Zn⁰ sites on plasma exposed ZnO samples after 24 hours of storage in air.³ This is not conclusive regarding the formation of reduced Zn during the CO₂ plasma exposure, though more sophisticated, air-free XPS methodologies may be necessary to observe them.

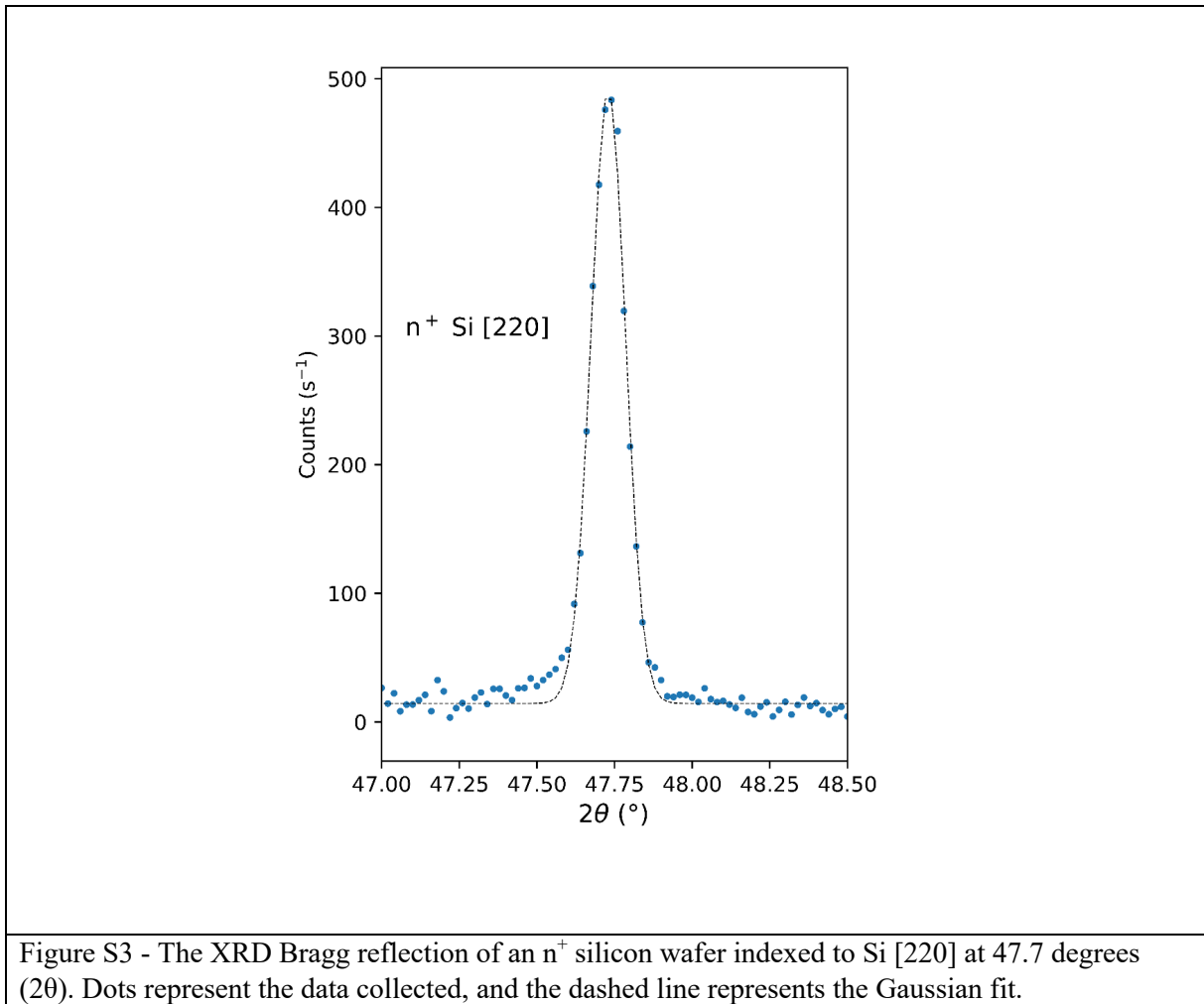


Figure S3 is an XRD measurement of a single crystal Si wafer substrate used to determine the instrumental broadening for calculating the Debye-Scherrer crystallite size of the TiO_2 and ZnO films. A Gaussian profile was fit to the data to determine the full width at half-maximum (FWHM) value for a practically infinitesimal-width single crystal Bragg reflection. This instrumental FWHM was subtracted from each FWHM determined for each sample from XRD measurements as shown in Equation S4 to determine the physical Debye-Scherrer broadening due to the characteristic grain size in the film.

Table S1. XRD derived crystallite size of as prepared, thermally annealed and plasma exposed ZnO films. Values were calculated using the ZnO peak indexed to the (0002) plane at $2\theta = 34.3^\circ$ degrees and Equations S1-S6.	
ZnO:	Crystallite Size (nm)
As prepared	15.53
Thermally annealed	24.61
CO ₂ Plasma	15.76
Ar Plasma	15.93

Table S1 lists the results of the XRD experiments performed on the ALD-ZnO samples as-prepared, after plasma exposure, and after thermal annealing. The difference in crystallite growth after plasma exposure, as compared to annealing, coupled with the low reactor temperature, Table S1, is consistent with the conclusion that the plasma exposure is not capable of inducing further crystallization and that changes to the morphology of the films can be attributed to plasma-surface interactions.

Table S2. XRD derived crystallite size of a thermally annealed TiO ₂ film. Values were calculated using the anatase TiO ₂ peak indexed to the (101) plane at $2\theta = 25.4^\circ$ and Equations S1-S3.	
TiO ₂ :	Crystallite Size (nm)
Thermally Annealed	18.71

Table S2 lists the results of XRD experiments performed on the ALD-TiO₂ samples after thermal annealing. The as prepared, CO₂ plasma and Ar plasma exposed samples were excluded as the films were found to be amorphous and an average crystallite size could not be determined.

- (1) Patterson, A. L. The Scherrer Formula for X-Ray Particle Size Determination. *Phys. Rev.* **1939**, *56* (10), 978–982. <https://doi.org/10.1103/PhysRev.56.978>.
- (2) Mehrabi, H.; Conlin, S. K.; Hollis, T. I.; Gattis, B. S.; Nelson Weker, J.; Coridan, R. H. Electrochemical Control of the Morphology and Functional Properties of Hierarchically Structured, Dendritic Cu Surfaces. *Energy Technol.* **2023**, *11* (3), 2201124. <https://doi.org/10.1002/ente.202201124>.
- (3) Morales, C.; Black, A.; Urbanos, F.; Granados, D.; Méndez, J.; Del Campo, A.; Yubero, F.; Soriano, L. Study of the Interface of the Early Stages of Growth under Quasi-Equilibrium Conditions of ZnO on Graphene/Cu and Graphite. *Adv. Mater. Interfaces* **2018**, *6*, 1801689. <https://doi.org/10.1002/admi.201801689>.